Research Paper
Computational Methods for Differential Equations
http://cmde.tabrizu.ac.ir
Vol. 14, No. 2, 2026, pp. 549-566
DOI:10.22034/cmde.2024.61722.2680

A monotonic weighted compact finite difference solution for a non-linear steady advection-diffusion equation

Prapol Chivapornthip*
Department of Industrial Engineering, Faculty of Engineering, Kasetsart University, Thailand.

Abstract

This paper introduces a monotonic weighted compact finite difference scheme (WC-FDM) designed to solve the non-linear one-dimensional steady advection-diffusion equation (ADE). The WC-FDM scheme is validated against the analytical solution and is adaptable to accommodate both uniform and non-uniform grid spacing. Criteria for selecting weights have been developed to ensure scheme monotonicity. Computational performance is benchmarked against other numerical schemes. Numerical analyses reveal that the WC-FDM accurately solves the non-linear steady ADE for both uniform and non-uniform grid spacing scenarios without introducing spurious oscillations. The proposed weight criteria maintain the monotonicity of the WC-FDM scheme resulting the computational stability regardless of the advection-dominance level and grid spacing uniformity.

Keywords. Compact finite difference, Monotonic scheme, Advection-diffusion, Weighted finite difference.
2010 Mathematics Subject Classification. 65L05, 34K06, 34K28.

1. Introduction

The robust solution of an advection-diffusion equation (ADE) presents a significant challenge in the field of computational fluid dynamics. Particularly, in scenarios where the ADE exhibits high advection dominance, conventional numerical solutions often yield spurious oscillations. To overcome this issue, a commonly employed approach is the use of consistently monotonic solutions such as the first-order upwind scheme. While the accuracy of the first-order upwind scheme is generally acceptable for advection-dominant instances of the ADE, its computational accuracy is significantly inferior to other non-monotonic numerical schemes when the equation leans towards diffusion dominance. Over the past decade, numerous numerical solutions capable of addressing both advection and diffusion dominance have been explored. Among the enduring solutions to suppress unwanted oscillations is the introduction of artificial viscosity [2, 19]. However, the artificial viscosity leads to the excessive dissipation of real physics resulting in the overly damped results [26]. Another classical method is the upwind scheme, often utilized with flux splitting approaches [2, 18]. However, while the first-order upwind scheme effectively preserves numerical stability in hyperbolic equations, it inherits accuracy limitations due to its low-order nature [18].

The accuracy of upwind schemes has been studied in several works. The computational performance of the upwind solution for wave equations in the second-order form was investigated in [4]. [3] shows that the central-upwind difference with predictor-corrector schemes outperform the traditional upwind backward scheme and achieve the same accuracy as the traditional artificial viscosity scheme when solving linear and non-linear dispersive Maxwell's equations. [24] incorporated a nodal Peclet number-based adaptive stencil approach to improve the accuracy of the upwind-radial basis function schemes. The computational accuracy of Godunov-based upwind schemes for the low Mach numbers condition was investigated in [28]. According to Godunov's theorem, while higher-order schemes improve accuracy, upwind schemes beyond first-order accuracy become non-monotonic, potentially leading to spurious oscillations in advection-dominated flows [5]. A study investigating the monotonic preservation of the Petrov-Galerkin upwind

Received: 20 May 2024; Accepted: 23 December 2024.
* Corresponding author. Email: prapol.c@ku.th.

scheme was undertaken by [5]. [13] investigated the stability limitations of second-order and third-order upwind schemes in semi-compressible gas flow. In the work of [34], total variation diminishing (TVD) schemes were employed to enforce monotonicity in numerical solutions by modifying solution's coefficients to adapt upwind schemes to meet TVD conditions. The polynomial upwind schemes with parameters controlling TVD have also been explored in [8].

All the numerical solutions as mentioned above are based on Taylor's series or polynomial equations. Apart from these approaches, alternative methods such as B-spline basis functions and exponential functions, have been investigated as numerical solutions for advection-diffusion problems. For instance, [10] introduced an exponential function-based upwind scheme. This approach has been used to solve both unsteady advection equations and Burger's equations in the space-time domain [10, 21]. Alternatively, [14] employed a quadratic B-spline shape function-based Finite Element Method (FEM) to solve the one-dimensional Burger's equation in the spatial domain. The cubic B-spline collocation method, combined with the Crank-Nicolson scheme, for solving the Burger's equation is discussed in [1]. In [20], a modified cubic B-spline basis functions were introduced, resulting in a numerically stable and diagonally dominant system. Furthermore, [27] proposed a combination of cubic B-spline and Runge-Kutta methods to address the two-dimensional Burger's equation. Extensions of B-spline collocation methods to quartic and septic degrees are detailed in [22, 23]. Despite the viability of B-spline basis functions as an alternative solution for the Burger's equation, ensuring accuracy in complex geometries remains challenging due to the strong dependence of basis function accuracy on the correlation of knots and interpolation points [35].

Several studies have shifted focus towards modifying Taylor's series-based finite difference methods to accommodate both advection and diffusion-dominated problems. One practical solution is the weighted finite difference method (WFDM). This method utilizes weights to alternate between or combine the first-order upwind scheme and the second-order central scheme based on the dominance of advection or diffusion. WFDM offers the advantage of producing monotonic and highly accurate results even with coarse grid points, across various levels of advection and diffusion when the appropriate value of weight is employed. For instance, [11] controlled scheme stability by using the weighted mean value of neighbouring points when encountering highly advective problems. Additionally, [9] approximated the advective term by combining weighted first-order upwind and central difference schemes. The study of [12] have demonstrated that WFDM with forward in time centered space (FTCS) outperforms the upwind-FTCS scheme. The concept of weighted schemes extends beyond switching between upwind and central schemes the spatial domain to encompass switching between explicit and implicit time schemes. In [29], the time derivative is approximated using a combination of weighted explicit and implicit schemes. This numerical scheme can adapt to classical explicit, classical implicit, and Crank-Nicolson schemes depending on the weight [29]. Further development of weighted schemes in the generalized finite difference method for two-dimensional advection-diffusion equations is discussed in [15]. While WFDM can provide unconditionally stable solutions for advection-dominated equations with few points, determining an appropriate weight for optimal results remains a significant challenge. Nonetheless, even without weights, the finite difference method can offer unconditionally stable solutions for advection-diffusion equations in several scenarios, particularly when formulated as compact finite difference schemes. Various studies have explored the application of compact finite difference schemes to non-linear ADEs. For example, [16, 17] developed a fourth-order compact finite difference solution using the Hopf-Cole transformation, while [25] extended the compact finite difference to sixth-order accuracy using the Runge-Kutta scheme in the time domain. Stability and convergence analyses of fourth-order compact finite difference solutions for one-dimensional Burger's equations can be found in [30]. Additionally, [36] introduced a MacCormack-based compact finite difference scheme, achieving fourth-order accuracy for both first-order and second-order derivatives. Finally, [32, 33] presented fourth-order compact finite difference schemes for transient three-dimensional Burger's equations.

This paper introduces a weighted compact finite difference method (WC-FDM), which is a consistently monotonic scheme. The aim is to develop a novel numerical solution for a non-linear advection-diffusion equation (ADE) that improves computational performance. The presented ADE equation describes the transport phenomena of uniaxial fluid flow within an axial geometry. The novelty of the proposed scheme lies in the combination of the first-order upwind scheme with the fourth-order compact finite difference method, alongside a weight selection algorithm that ensures monotonicity under varying levels of advection dominance. This method can accommodate both uniform and non-uniform grid spacing. The computational accuracy of the proposed numerical scheme is validated against the

analytical solution presented by [31], the upwind-central difference scheme, full central difference scheme, and full fourth-order compact difference scheme.

2. Mathematical model

The non-linear one-dimensional steady ADE is defined as follows.

$$u\partial_x u - \nu\partial_x^2 u = 0, \quad x \in R^{[-1,1]}, \tag{2.1}$$

where u is a fluid velocity, ν is a diffusivity. The boundary conditions for Eq. (2.1).

$$u(-1) = 1.01, \tag{2.2}$$

$$u(1) = -1. \tag{2.3}$$

The analytical solution for Eq. (2.1) based on [31] is shown as follows.

$$u(x) = -C_1 \tanh\left[\frac{C_1}{2\nu}(x - C_2)\right], \tag{2.4}$$

$$C_1(2+\delta) = \left(C_1^2 + \delta + 1\right)\tanh\left(\frac{C_1}{\nu}\right), \tag{2.5}$$

$$C_2 = 1 - \frac{2\nu}{C_1}\tanh^{-1}\left(\frac{1}{C_1}\right). \tag{2.6}$$

The velocity profile from Eq. (2.4) can be calculated using the constants defined in Eqs. (2.5) and (2.6). Since Eq. (2.5) is the non-linear equation, the constant C_1 can be determined through the iterative method. Subsequently, the constant C_2 is solved from Eq. (2.6).

3. Weighted Compact Finite Difference

The governing Equation (2.1) can be solved by approximating the first and second derivatives using a weighted compact finite difference. The proposed method combines the first-order upwind scheme with the fourth-order compact scheme. The first derivative, $\partial_x u$, is evaluated using a weighted combination of the first-order upwind scheme and the fourth-order compact scheme centred on the stencil's central point. While, the second derivative, $\partial_x^2 u$, is evaluated separately using the fourth-order compact scheme centred on the stencil's central point. The approximation solution of Eq. (2.1) can be formulated as follows

$$u\left[(1-\omega)\left(a^+\partial_x u^- + a^-\partial_x u^+\right) + \omega\partial_x u^0\right] - \nu\partial_x^2 u = 0, \tag{3.1}$$

$$a^+ = \frac{\max(0,u)}{u}, \quad a^- = \frac{\min(0,u)}{u}. \tag{3.2}$$

It is well known that the first-order upwind exhibits a superior numerical stability, but lacks high-order accuracy. On the other hands, the compact scheme offers great approximation accuracy but can produce oscillatory results at a high degree of advection. The proposed scheme uses the weight $\omega \in \mathbb{R}^{[0,1]}$ to control the scheme's stability and accuracy by switching between or combining the first-order upwind scheme and the fourth-order compact scheme according to the level of advection. The selection of the weight, ω, is discussed later in section 4. The parameters, $a^+ \in \{0,1\}$ and $a^- \in \{0,1\}$, represent the functions switching between first order backward or forward differences based on the direction of the velocity u. Specially, when $u > 0$ and $a^+ = 1$, $\partial_x u$ is approximated by the first-order backward difference or vice versa. When $u = 0$, the governing Equation (2.1) transforms into a pure diffusion problem, where switching function (3.2) eliminates all upwind schemes, leaving only the central difference to be solved. The first derivatives $\partial_x u^-$ and $\partial_x u^+$ correspond to the first order backward difference and forward difference, respectively.

$$\partial_x u^- = \frac{u_i - u_{i-1}}{h_{i-1}}, \tag{3.3}$$

$$\partial_x u^+ = \frac{u_{i+1} - u_i}{h_{i+1}}, \tag{3.4}$$

$$h_{i-1} = x_i - x_{i-1}, \quad h_{i+1} = x_{i+1} - x_i. \tag{3.5}$$

The first derivative $\partial_x u^0$ and the second derivative $\partial_x^2 u$ based on central-point approach are approximated by the compact finite difference. Differentiating Eq. (2.1) up to the third and fourth orders and assuming velocity u multiplied by the first-derivative term as a constant yields:

$$u\partial_x^2 u - \nu\partial_x^3 u = 0, \tag{3.6}$$
$$u\partial_x^3 u - \nu\partial_x^4 u = 0. \tag{3.7}$$

Expanding the Taylor's series expansion up to the fourth-order term based on points u_{i-1} and u_{i+1} results in:

$$u_{i+1} = u_i + h_{i+1}\partial_x u + \frac{h_{i+1}^2}{2}\partial_x^2 u + \frac{h_{i+1}^3}{6}\partial_x^3 u + \frac{h_{i+1}^4}{24}\partial_x^4 u, \tag{3.8}$$
$$u_{i-1} = u_i - h_{i-1}\partial_x u + \frac{h_{i-1}^2}{2}\partial_x^2 u - \frac{h_{i-1}^3}{6}\partial_x^3 u + \frac{h_{i-1}^4}{24}\partial_x^4 u. \tag{3.9}$$

Substituting Eqs. (3.6)–(3.7) into Eqs. (3.8)–(3.9) and solving for $\partial_x u^0$ and $\partial_x^2 u$ results in the compact central scheme, as follows.

$$\partial_x u^0 = \frac{u_{i+1}G_{i-1} - u_i\left(G_{i-1} - G_{i+1}\right) - u_{i-1}G_{i+1}}{D}, \tag{3.10}$$
$$\partial_x^2 u = \frac{u_{i+1}h_{i-1} - u_i\left(h_{i-1} + h_{i+1}\right) + u_{i-1}h_{i+1}}{D}, \tag{3.11}$$
$$G_{i-1} = \frac{h_{i-1}^2}{2} - \frac{u_i h_{i-1}^3}{6\nu} + \frac{u_i^2 h_{i-1}^4}{24\nu^2}, \tag{3.12}$$
$$G_{i+1} = \frac{h_{i+1}^2}{2} + \frac{u_i h_{i+1}^3}{6\nu} + \frac{u_i^2 h_{i+1}^4}{24\nu^2}, \tag{3.13}$$
$$D = h_{i+1}G_{i-1} + h_{i-1}G_{i+1}. \tag{3.14}$$

Substituting Eqs. (3.3), (3.4), (3.10), and (3.11) into the governing Equation (2.1) results in the approximation solution based on the 3-point stencil as follows.

$$c_{i-1}u_{i-1} + c_i u_i + c_{i+1}u_{i+1} = 0, \tag{3.15}$$
$$c_{i-1} = -a^+\frac{u_i\left(1-\omega\right)}{h_{i-1}} - \frac{\omega u_i G_{i+1} + \nu h_{i+1}}{D}, \tag{3.16}$$
$$c_i = u_i\left(1-\omega\right)\left(\frac{a^+}{h_{i-1}} - \frac{a^-}{h_{i+1}}\right) + \frac{\omega u_i\left(G_{i+1} - G_{i-1}\right) + \nu h_{i+1} + \nu h_{i-1}}{D}, \tag{3.17}$$
$$c_{i+1} = a^-\frac{u_i\left(1-\omega\right)}{h_{i+1}} + \frac{\omega u_i G_{i-1} - \nu h_{i-1}}{D}. \tag{3.18}$$

4. Monotonicity criteria for weighted compact finite difference

The proposed method yields stable or non-oscillatory results when Eq. (3.15) becomes a monotonic function. To obtain a consistent monotonic solution at any level of advection, both coefficients c_{i-1} and c_{i+1} of Eq. (3.15) must have the same sign [6]. The weight, ω, is a key parameter for controlling the sign of both coefficients c_{i-1} and c_{i+1}. The sign analysis begins with evaluating the signs of the numerators and the denominators in Eqs. (3.16) and (3.18). Initially, Eqs. (3.12) and (3.13) are rearranged to express them as a function of u_i, as follows.

$$G_{i-1} = f_{i-1}\left(u_i\right) = d_{i-1} + b_{i-1}u_i + a_{i-1}u_i^2, \tag{4.1}$$
$$G_{i+1} = f_{i+1}\left(u_i\right) = d_{i+1} + b_{i+1}u_i + a_{i+1}u_i^2, \tag{4.2}$$
$$a_{i-1} = \frac{h_{i-1}^4}{24\nu^2}\ ,\quad a_{i+1}=\frac{h_{i+1}^4}{24\nu^2}\ ,\quad b_{i-1} = -\frac{h_{i-1}^3}{6\nu}\ ,\quad b_{i+1} = \frac{h_{i+1}^3}{6\nu}\ ,\quad d_{i-1} = \frac{h_{i-1}^2}{2}\ ,\quad d_{i+1} = \frac{h_{i+1}^2}{2}. \tag{4.3}$$

From Eqs. (4.1) and (4.2), we observe that $f_{i+1}(u_i)$ and $f_{i-1}(u_i)$ represent the quadratic equations with u_i as variable. Calculating the discriminants of functions (4.1) and (4.2) reveals that:

$$-\frac{h_{i-1}^6}{18\nu^2} < 0, \tag{4.4}$$

$$-\frac{h_{i+1}^6}{18\nu^2} < 0. \tag{4.5}$$

Eqs. (4.4) and (4.5) indicate that G_{i-1} and G_{i+1} have only one sign, either positive or negative, across the change of velocity u_i. To calculate the exact sign of G_{i-1} and G_{i+1}, the functions (4.1) and (4.2) are differentiated with respect to u_i to obtain the location of the deflection point.

$$\partial_{u_i} f_{i-1} = -\frac{h_{i-1}^3}{6\nu} + \frac{u_i h_{i-1}^4}{12\nu^2} = 0, \tag{4.6}$$

$$\partial_{u_i} f_{i+1} = \frac{h_{i+1}^3}{6\nu} + \frac{u_i h_{i+1}^4}{12\nu^2} = 0. \tag{4.7}$$

From the above two expressions, we can find the velocity u_i at the deflection point of Eqs. (4.1) and (4.2) as follows.

$$u_i = \begin{cases} \frac{2\nu}{h_{i-1}}, & \text{for } f_{i-1}(u_i), \\ -\frac{2\nu}{h_{i+1}}, & \text{for } f_{i+1}(u_i). \end{cases} \tag{4.8}$$

Eq. (4.8) is substituted into (4.1) and (4.2) to estimate the signs of f_{i-1} and f_{i+1} at the deflection point, resulting in:

$$f_{i-1}\left(\frac{2\nu}{h_{i-1}}\right) = \frac{h_{i-1}^2}{3} > 0, \tag{4.9}$$

$$f_{i+1}\left(-\frac{2\nu}{h_{i+1}}\right) = \frac{h_{i+1}^2}{3} > 0. \tag{4.10}$$

Eqs. (4.9) and (4.10) show that the functions f_{i-1} and f_{i+1} are positive at the deflection point and therefore (Figure 1),

$$\begin{cases} G_{i-1} > 0, & \forall\ u_i \in \mathbb{R}, \\ G_{i+1} > 0, & \forall\ u_i \in \mathbb{R}. \end{cases} \tag{4.11}$$

According to Eq. (4.11), $h_{i-1} > 0$, and $h_{i+1} > 0$, therefore, the denominator:

$$D > 0,\ \forall\ u_i \in \mathbb{R}. \tag{4.12}$$

However, the numerators of coefficients c_{i-1} and c_{i+1} in Eqs. (3.16) and (3.18) respectively may have uncertain signs depending on the direction of u_i. For $\omega \in [0,1]$ and $u_i > 0$, the coefficient $c_{i-1} < 0$, while the sign of coefficient c_{i+1} can fluctuate depending on the right-hand side terms of Eq. (3.18). To maintain the monotonicity of the scheme or to ensure that the sign of coefficient c_{i+1} is also negative, the weight ω is utilized to force the coefficient c_{i+1} to be negative according to the following condition.

$$\omega \le \frac{\nu h_{i-1}}{|u_i|\, G_{i-1}}. \tag{4.13}$$

In similar fashion, for $\omega \in [0,1]$ and $u_i < 0$, the coefficient $c_{i+1} < 0$, while the sign of coefficient c_{i-1} can fluctuate. The weight ω that maintains the monotonic scheme must ensure that $c_{i-1} < 0$. This weight ω is:

$$\omega \le \frac{\nu h_{i+1}}{|u_i|\, G_{i+1}}. \tag{4.14}$$

The weight criteria (4.13) and (4.14) demonstrate that the weight ω is always positive since $\nu > 0$, $h_{i-1} > 0$, $h_{i+1} > 0$, $G_{i-1} > 0$, and $G_{i+1} > 0$. However, selecting the weight ω based on Eqs. (4.13) and (4.14) is still n ambiguous task since it can be any arbitrary value that satisfies Eqs. (4.13) and (4.14) and falls within the range between zero to one.

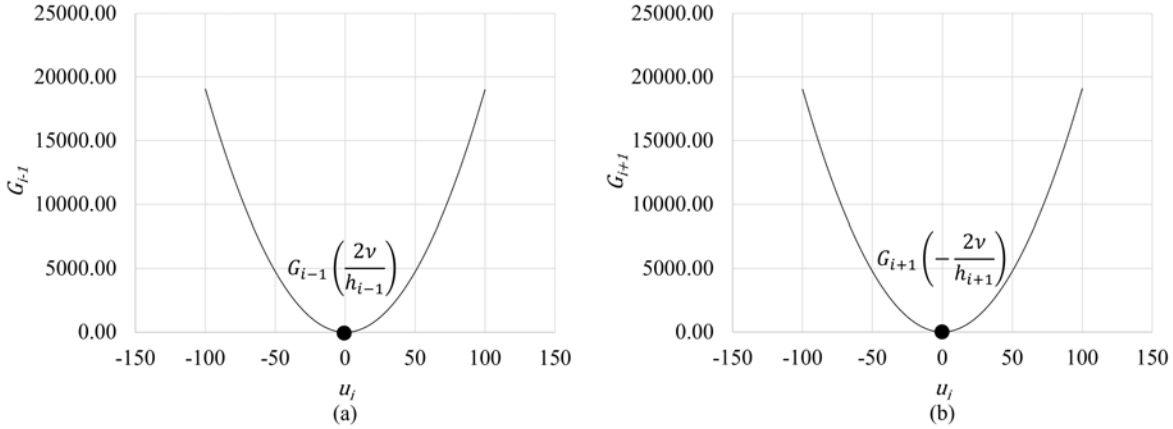

FIGURE 1. Example profiles of G_{i-1} and G_{i+1} along the velocity u_i with $h_{i-1} = h_{i+1} = 0.26$ and $\nu = 0.01$ a) indicates the deflection point of G_{i-1} at $u_i = 2\nu/h_{i-1}$ and b) indicates the deflection point of G_{i+1} at $u_i = -2\nu/h_{i+1}$.

Therefore, it is more convenient to select a specific value of the weight ω that at least initiates a monotonic scheme. In such case, the weight ω is set to its maximum value of Eqs. (4.13) and (4.14).

$$\omega = \begin{cases} \frac{\nu h_{i-1}}{|u_i| G_{i-1}}, & \forall\ u_i > 0, \\ \frac{\nu h_{i+1}}{|u_i| G_{i+1}}, & \forall\ u_i < 0. \end{cases} \tag{4.15}$$

5. Computational Processes

In this work, the Newton-Raphson iterative method is employed to solve Eq. (3.15), a non-linear equation with multiple variables u_{i-1}, u_i, and u_{i+1}. The iterative solution begins by formulating the weighted compact finite difference as a vector-valued function $\mathbf{f}$ of the initialized velocities vector $\mathbf{u}^{(k)} = (u_1, u_2, u_3, \ldots, u_n)^{(k)}$ in the matrix form, as follows.

$$\mathbf{f}\left(\mathbf{u}^{(k)}\right) = \begin{bmatrix} 0 \\ c_1u_1 + c_2u_2 + c_3u_3 \\ c_2u_2 + c_3u_3 + c_4u_4 \\ \vdots \\ c_{n-2}u_{n-2} + c_{n-1}u_{n-1} + c_nu_n \\ 0 \end{bmatrix} = \begin{bmatrix} 0 \\ 0 \\ 0 \\ \vdots \\ 0 \\ 0 \end{bmatrix}, \tag{5.1}$$

where the superscript k denotes the iteration number. The first and the last rows of Eq. (5.1) are replaced by zero, enabling Eq. (5.1) to meet the boundary conditions (2.2) and (2.3). The predicted velocities u_i at the next iteration number, $k+1$, can be calculated according to the following expression.

$$\mathbf{u}^{(k+1)} = \mathbf{u}^{(k)} - \left(\mathrm{d}\mathbf{f}\left(\mathbf{u}^{(k)}\right)\right)^{-1} \mathbf{f}\left(\mathbf{u}^{(k)}\right), \tag{5.2}$$

where the Jacobian matrix $\mathrm{d}\mathbf{f}\left(\mathbf{u}^{(k)}\right)$ is

$$\mathrm{df}\left(\mathbf{u}^{(k)}\right)=\begin{bmatrix} 1 & 0 & 0 & & \dots & 0 \\ c_1 & \partial_{u_2}\left(c_2u_2\right) & c_3 & & \dots & 0 \\ 0 & c_2 & \partial_{u_2}\left(c_3u_3\right) & c_4 & & 0 \\ \vdots & \vdots & \vdots & \ddots & & \vdots \\ & & & c_{n-2} & \partial_{u_{n-1}}\left(c_{n-1}u_{n-1}\right) & c_n \\ 0 & \dots & & 0 & 0 & 1 \end{bmatrix}_{n\times n}, \tag{5.3}$$

$$\begin{aligned} \partial_{u_i}\left(c_iu_i\right) &= c_i+u_i\left(1-\omega\right)\left(\frac{a^+}{h_{i-1}}-\frac{a^-}{h_{i+1}}\right)-\omega u_i^2\left(\frac{\left(\partial_xG_{i-1}-\partial_xG_{i+1}\right)}{D}+\left(G_{i-1}-G_{i+1}\right)\partial_x\left(\frac{1}{D}\right)\right) \\ &\quad -\frac{\omega u_i\left(G_{i-1}-G_{i+1}\right)}{D}+\nu u_i\left(h_{i-1}+h_{i+1}\right)\partial_x\left(\frac{1}{D}\right), \\ \partial_{u_i}G_{i-1} &= \frac{u_ih_{i-1}^4}{12\nu^2}-\frac{h_{i-1}^3}{6\nu}, \\ \partial_{u_i}G_{i+1} &= \frac{u_ih_{i+1}^4}{12\nu^2}+\frac{h_{i+1}^3}{6\nu}, \\ \partial_x\left(\frac{1}{D}\right) &= -\frac{h_{i+1}\partial_{u_i}G_{i-1}+h_{i-1}\partial_{u_i}G_{i+1}}{D^2}. \end{aligned} \tag{5.4}$$

The diagonal components of the first and the last rows of Eq. (5.3) are set to one, enabling Eq. (5.3) to meet the boundary conditions (2.2) and (2.3). The weight criteria from Eqs. (4.13) and (4.14) are still valid to control the monotonicity of Eq. (5.3) since coefficients c_{i-1} and c_{i+1} remain unchanged. The iterative solution in Eq. (5.2) continues until the difference between the velocities vector $\mathbf{u}^{(k+1)}$ and $\mathbf{u}^{(k)}$ reaches the specified tolerance.

6. Convergence Analysis

The convergence of the proposed numerical method is evaluated in terms of the order of convergence which can be calculated as follows [7].

$$\frac{\|\mathbf{u}-\mathbf{u_A}\|_2}{\|\mathbf{u_A}\|_2}=Cn^{-p}. \tag{6.1}$$

where $\mathbf{u}$ is the velocity vector calculated by the proposed numerical method, $\mathbf{u_A}$ is the velocity vector calculated by the analytical solution (2.4)–(2.6), C is the constant and p is the order of convergence. Eq. (6.1) is linearised by taking natural logarithm on both sides.

$$\ln C\ -p\ln n\ =\ln\left(\frac{\|\mathbf{u}-\mathbf{u_A}\|_2}{\|\mathbf{u_A}\|_2}\right). \tag{6.2}$$

The order of convergence, p, can be solved from Eq. (6.2) using the least square method.

7. Results and discussion

Numerical analysis is conducted under two simulation scenarios: the uniform grid spacing and the non-uniform grid spacing. Both scenarios simulate the non-linear ADEs with respect to the boundary conditions (2.2) and (2.3), the iteration termination tolerance based on the relative root mean square error (RRMSE), and five diffusivities ν as presented in Table 1. The computational performance of the proposed weighted-compact finite difference (WC-FDM) is benchmarked against the upwind scheme (Upwind), where the first-order term is approximated by the first-order backward difference and the second-order term by the central difference. Additionally, the comparisons are made with

the conventional second-order central scheme (Central), where both first and second-order terms are approximated by the second-order central difference, and the fourth-order compact finite difference (Compact), considering a varying number of points n. The uniform and non-uniform grid spacing scenarios are formulated as follows.

For uniform grid spacing:

$$x = \frac{2\,(i-1)}{n-1} - 1, \tag{7.1}$$

For non-uniform grid spacing:

$$x = \begin{cases} \frac{1.3(i-1)}{0.3n-1} - 1, & \forall\ i \in \mathbb{N}^{[1,0.3n]}, \\ \frac{0.7(i-0.3n)}{0.7n} + 0.3, & \forall\ i \in \mathbb{N}^{[0.3n,n]}. \end{cases} \tag{7.2}$$

Numerical simulation results of the uniform grid spacing are presented in Figures 2–5, while those for the non-uniform grid spacing is presented in Figures 6–9. In the non-uniform grid spacing scenario, the point density within the range $i \in \mathbb{N}^{[1,0.3n]}$ is smaller than the point density in the range $i \in \mathbb{N}^{[0.3n,n]}$.

TABLE 1. Simulation parameters.

Parameters	**Value**
Iteration termination tolerance (RRMSE)	10^{-9}
Diffusivities ν	0.1, 0.05, 0.025, 0.01
Number of points n	20, 40, 80, 160, 320, 640

Figures 2–5 compare the proposed numerical scheme (WC-FDM) with other numerical schemes in a uniform grid spacing scenario. Figure 2 demonstrates that all schemes provide stable solutions at high diffusion levels ($\nu = 0.1$ and 0.05). However, the upwind scheme (Upwind) shows the lowest computational accuracy at these diffusivities (Figures 2(a) and (b)), due to its first-order accuracy in approximating the advection term. In contrast, other schemes use higher-order approximations for the advection term.

At lower diffusion levels ($\nu = 0.025$ and 0.01), the central scheme (Central) exhibits spurious oscillations. These oscillations arise because the central scheme's approximation of the advection and diffusion terms result in non-monotonic solutions. Similarly, the compact scheme (Compact) also shows small oscillations at $\nu = 0.01$, leading to lower accuracy compared to both the WC-FDM and upwind schemes. This indicates that the compact scheme becomes non-monotonic with a smaller stencil size in advection-dominant problems. However, when the stencil size is increased, the spurious oscillations of both the compact and central schemes vanish, and the solutions become monotonic (Figures 3(a)–(d)).

The WC-FDM and upwind schemes maintain numerical stability across all diffusion levels (Figures 2(a)–(d) and Figures 3 (a)–(d)) because both are consistently monotonic. The WC-FDM scheme demonstrates a notable advantage over the upwind scheme, achieving superior computational accuracy at high diffusion levels ($\nu = 0.1$ and 0.05) and matching the upwind scheme's accuracy at low diffusion levels ($\nu = 0.025$ and 0.01) or when the problem becomes highly advection-dominant. This advantage is due to the weight criteria incorporated in the WC-FDM, which effectively eliminates numerical oscillations in highly advection-dominated scenarios while preserving high accuracy in more diffusive contexts.

Figure 4 illustrates the convergence of all numerical schemes based on the relative root mean square error (RRMSE) as a function of stencil size. The RRMSE of all schemes converges to an asymptote, except for the upwind scheme, which shows slight divergence at very fine stencils ($n = 640$) (Figure 4(d)). This divergence may be related to the non-linearity of the governing equations, where computational accuracy is sensitive to changes in discretization. This sensitivity is evident in Figure 4(c), where the compact scheme shows a slight overshoot at $n = 40$. In contrast, the WC-FDM scheme handles this discretization error sensitivity effectively, with the RRMSE decreasing rapidly across all stencil sizes and diffusion levels (Figures 4(a)–(d)). The weight criteria in Eq. (4.15) allow the WC-FDM scheme to behave like a full compact scheme at high diffusion levels ($\nu = 0.1$ and 0.05) and like a full upwind scheme in more highly advection-dominated scenarios, ensuring accurate and stable solutions.

Figure 5 compares the computational speed of all schemes by the number of iterations required to achieve a steady-state solution at an error tolerance of 10^{-9} RRMSE. The upwind scheme requires more iterations as the stencil size increases, while other higher-order schemes eventually reach a steady-state when the discretized domain exceeds 160 points. Overall, the WC-FDM scheme has a computational speed comparable to the compact scheme across all diffusion levels and outperforms the compact scheme at $\nu = 0.025$ and 0.01 with smaller stencil sizes (Figures 5(c) and (d)).

Tables 2–4 summarize the overall computational performance of the WC-FDM scheme. Both the WC-FDM and compact schemes show minimal errors at $\nu = 0.1$ across varying numbers of points (Table 2), with nearly identical convergence rates, the highest among the compared schemes (Table 4). Conversely, the upwind scheme shows the largest error due to its first-order accuracy, which is insufficient for precisely approximating the given non-linear advection-diffusion equation. In highly advection-dominant cases ($\nu = 0.01$), both the WC-FDM and upwind schemes demonstrate the best accuracy within the 20–40 point range (Table 3). Beyond this range, other schemes outperform the upwind scheme. The WC-FDM, with its proposed weight criteria, consistently exhibits minimal errors across both diffusion levels and stencil sizes, combining the advantages of both upwind and compact schemes.

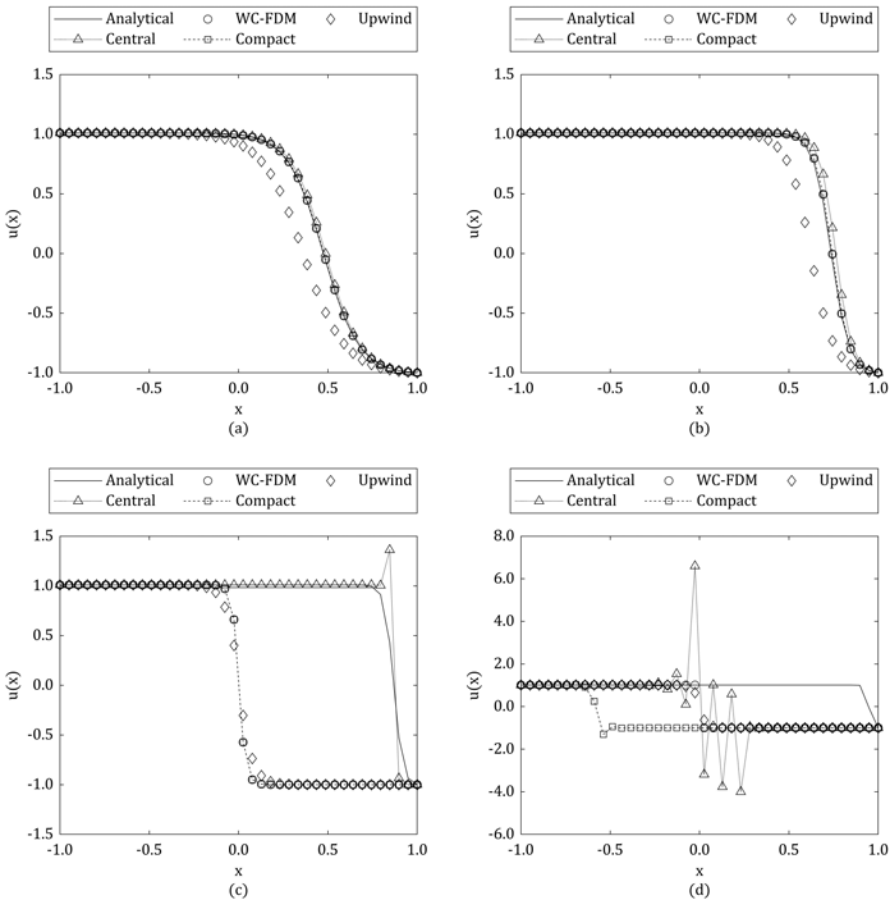

FIGURE 2. Numerical simulation results of the non-linear steady ADE with 40 uniformly spaced grid points at different diffusivities a) $\nu = 0.1$, b) $\nu = 0.05$, c) $\nu = 0.025$, and d) $\nu = 0.01$.

The computational accuracy of all schemes significantly decreases in the non-uniform grid spacing scenario (Figures 6–8 and Tables 5–6). Notably, the variation in grid spacing across the spatial domain affects the computational accuracy

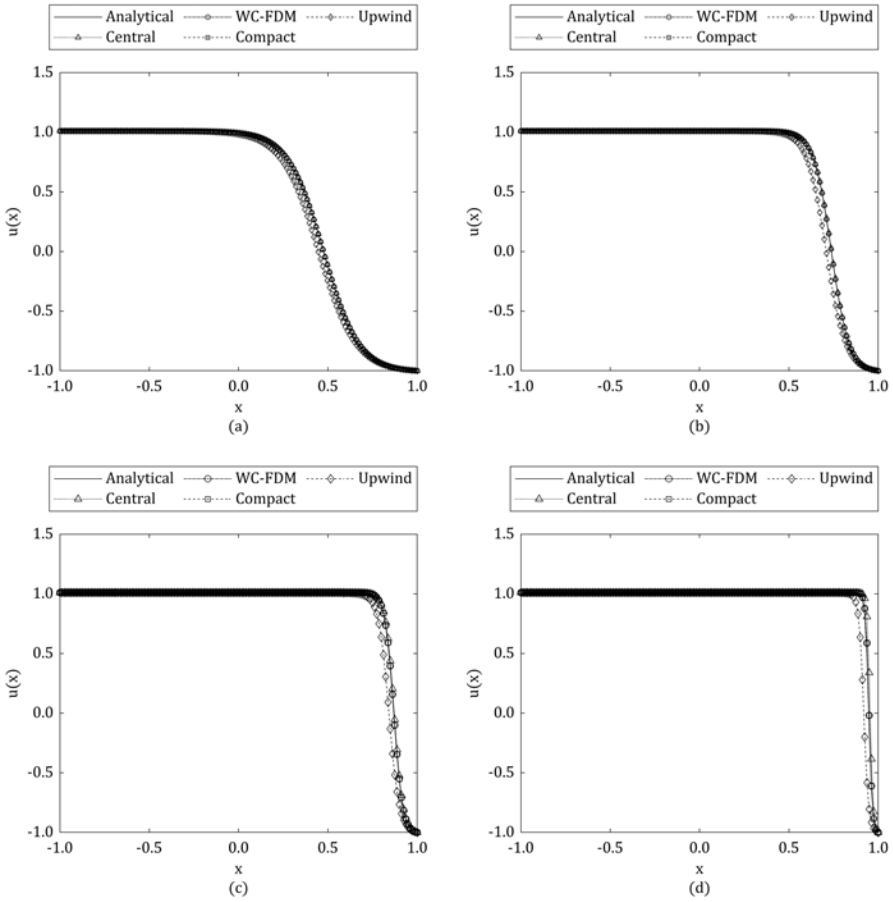

FIGURE 3. Numerical simulation results of the non-linear steady ADE with 160 uniformly spaced grid points at different diffusivities a) $\nu = 0.1$, b) $\nu = 0.05$, c) $\nu = 0.025$, and d) $\nu = 0.01$.

of all schemes. Particularly, oscillations are evident in the compact scheme (Compact) (Figures 6(c) and (d)), revealing that the compact scheme cannot maintain the monotonic property even in highly advection-dominant problems. Meanwhile, the WC-FDM and upwind schemes (Upwind) maintain their stability. The first-order approximation of the upwind scheme always gives a monotonic solution, which is independent of the stencil size, grid spacing, and diffusion level. In contrast, the monotonicity of the WC-FDM is maintained by the proposed weight criteria. Figures 6 and 7 demonstrate that the proposed weight criteria can effectively stabilize the solution even with the non-uniform grid spacing scenario.

In addition, the non-uniform grid spacing affects the order of convergence, and the number of iterations required to reach a steady state result. This spacing results in the lower computational accuracy for all schemes, which in turn decreases the order of convergence and increases the number of iterations (Table 7, and Figures 8–9). Unlike uniform grid spacing scenario, it is difficult to predict the order of convergence in the non-uniform scenario, as solution accuracy depends on the uniformity of grid spacing and the non-linearity. However, the WC-FDM scheme can still maintain the order of convergence above two in such scenarios, even though the scheme is partially based on the central point approximation. This contrasts with the full central scheme, which exhibits the diverging order of convergence (Table 7) when the variation of grid spacing is significant, especially in highly diffusion-dominant scenario ($\nu = 0.1$ and $\nu = 0.05$).

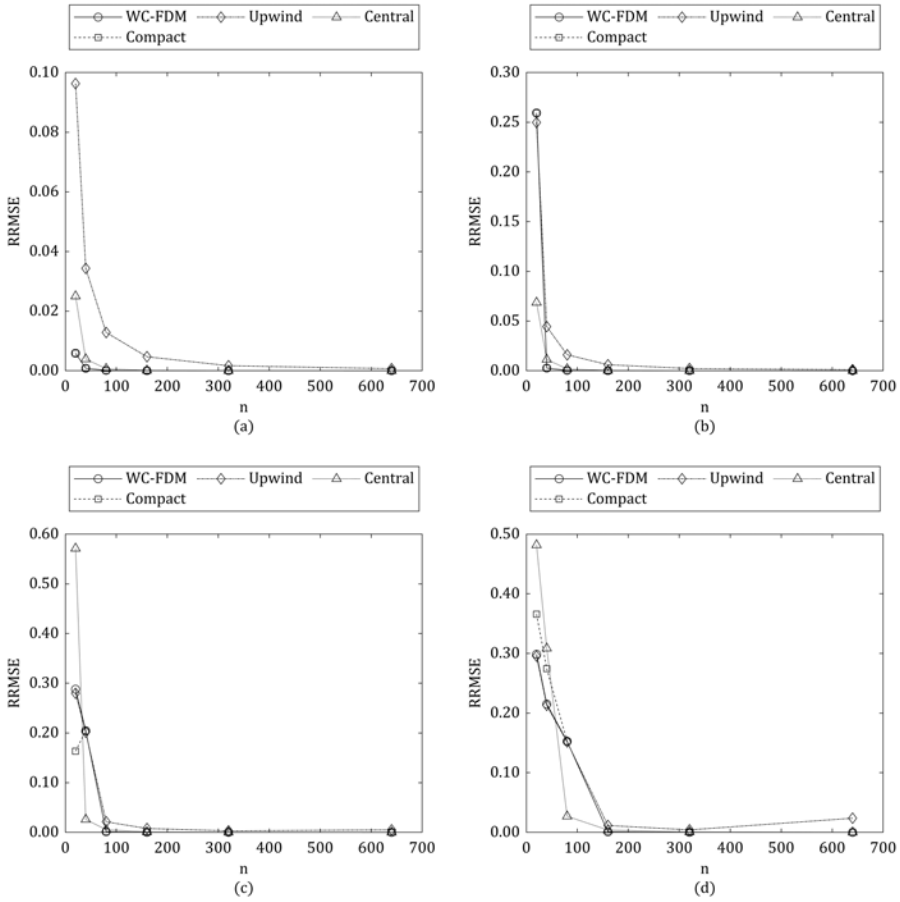

FIGURE 4. Error convergence of the numerical schemes with uniform grid point spacing at different diffusivities a) $\nu = 0.1$, b) $\nu = 0.05$, c) $\nu = 0.025$, and d) $\nu = 0.01$.

TABLE 2. The computational performance of the numerical schemes with diffusivity $\nu = 0.1$ and uniform grid spacing.

		Number of points					
Error	Schemes	20	40	80	160	320	640
L^∞ norm error	WC-FDM	0.066913	0.013886	0.003273	0.000799	0.000195	0.000044
	Upwind	0.977572	0.524857	0.283027	0.147321	0.075197	0.043590
	Central	0.297163	0.063575	0.015189	0.003725	0.000922	0.000226
	Compact	0.066913	0.013886	0.003273	0.000799	0.000195	0.000044
MAPE (%)	WC-FDM	53.5732	0.9287	0.2512	0.0705	0.0195	0.0049
	Upwind	605.0191	38.0521	24.4506	14.9364	8.7468	5.7681
	Central	240.5525	4.8151	1.3262	0.3775	0.1065	0.0295
	Compact	53.5732	0.9287	0.2512	0.0705	0.0195	0.0049
RRMSE	WC-FDM	5.88E-03	8.18E-04	1.35E-04	2.33E-05	4.03E-06	6.43E-07
	Upwind	9.63E-02	3.43E-02	1.28E-02	4.69E-03	1.69E-03	6.91E-04
	Central	2.50E-02	3.92E-03	6.68E-04	1.17E-04	2.04E-05	3.55E-06
	Compact	5.88E-03	8.18E-04	1.35E-04	2.33E-05	4.03E-06	6.43E-07

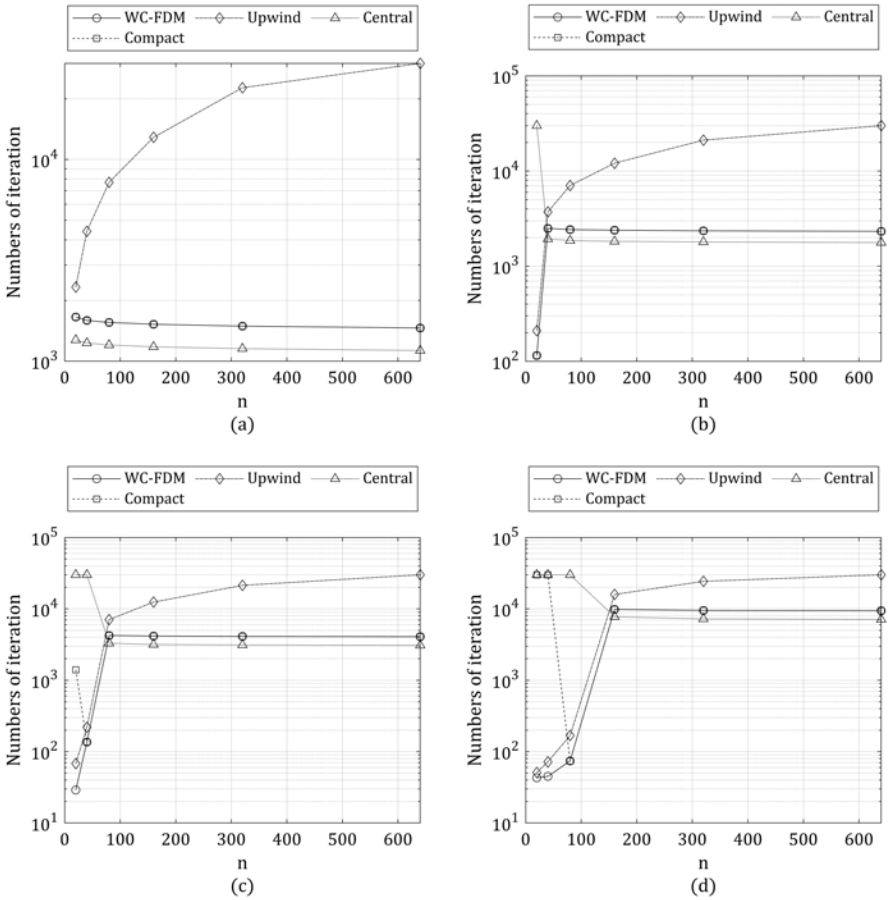

FIGURE 5. Number of iterations of the numerical schemes required to obtain the steady velocity with uniform grid point spacing at different diffusivities a) $\nu = 0.1$, b) $\nu = 0.05$, c) $\nu = 0.025$, and d) $\nu = 0.01$.

TABLE 3. The computational performance of the numerical schemes with diffusivity $\nu = 0.01$ and uniform grid spacing.

		Number of points					
Error	Schemes	20	40	80	160	320	640
L^∞ norm error	WC-FDM	2.010000	2.010000	2.010000	0.101022	0.021372	0.005051
	Upwind	2.010000	2.010000	2.010000	1.070471	0.614883	2.009669
	Central	4.879184	5.588293	1.876112	0.450103	0.096249	0.023282
	Compact	3.420107	2.311134	2.010000	0.101022	0.021372	0.005051
MAPE (%)	WC-FDM	89.6027	127.1196	104.3011	0.7273	0.1172	0.0398
	Upwind	89.5867	127.0910	104.2451	7.2446	3.6787	27.7631
	Central	189.9909	156.1783	16.4079	3.3774	0.5936	0.2093
	Compact	126.3026	184.6779	104.3011	0.7273	0.1172	0.0398
RRMSE	WC-FDM	0.298645	0.215097	0.152570	0.000927	0.000129	0.000021
	Upwind	0.295511	0.212893	0.151451	0.011514	0.004172	0.023713
	Central	0.481839	0.308611	0.026952	0.003926	0.000608	0.000104
	Compact	0.365897	0.274415	0.152570	0.000927	0.000129	0.000021

TABLE 4. The order of convergence p for the numerical schemes with uniform grid spacing.

	Order of convergence p			
Schemes	$\nu = 0.1$	$\nu = 0.05$	$\nu = 0.025$	$\nu = 0.01$
WC-FDM	2.6093	3.1940	3.4165	3.0967
Upwind	1.4313	1.5409	1.3912	1.1126
Central	2.5483	2.5615	2.7663	2.5894
Compact	2.6093	3.1940	3.2996	3.1686

TABLE 5. The computational performance of the numerical schemes with diffusivity $\nu = 0.1$ and non-uniform grid spacing.

		Number of points					
Error	Schemes	20	40	80	160	320	640
L^∞ norm error	WC-FDM	1.46E+00	1.31E+00	1.25E-01	2.16E-02	5.04E-03	1.24E-03
	Upwind	1.62E+00	1.81E+00	1.75E+00	1.65E+00	1.47E+00	9.77E-01
	Central	1.10E+00	9.16E-01	1.66E+01	5.04E-01	7.27E+04	2.01E+00
	Compact	1.46E+00	1.31E+00	1.25E-01	2.16E-02	5.04E-03	1.24E-03
MAPE (%)	WC-FDM	1.31E+02	6.28E+03	4.36E+02	3.96E+01	5.15E+00	7.76E-01
	Upwind	1.48E+02	6.82E+03	3.49E+03	1.82E+03	9.92E+02	4.99E+02
	Central	1.19E+02	5.18E+03	5.54E+04	8.63E+02	2.03E+07	6.91E+02
	Compact	1.31E+02	6.28E+03	4.36E+02	3.96E+01	5.15E+00	7.76E-01
RRMSE	WC-FDM	1.76E-01	1.17E-01	8.56E-03	1.05E-03	1.73E-04	3.00E-05
	Upwind	2.13E-01	1.64E-01	1.10E-01	7.27E-02	4.63E-02	2.27E-02
	Central	1.55E-01	8.51E-02	1.84E+00	2.42E-02	1.77E+03	5.74E-02
	Compact	1.76E-01	1.17E-01	8.56E-03	1.05E-03	1.73E-04	3.00E-05

TABLE 6. The computational performance of the numerical schemes with diffusivity $\nu = 0.01$ and non-uniform grid spacing.

		Number of points					
Error	Schemes	20	40	80	160	320	640
L^∞ norm error	WC-FDM	2.010000	2.010000	2.010000	2.010000	2.010000	0.001228
	Upwind	2.009949	2.009999	1.054593	0.612213	0.342437	0.180862
	Central	5.312704	3.937002	2.300301	2.855492	20.333375	2.010000
	Compact	2.011044	2.010000	4.578367	2.010000	2.010000	0.001228
MAPE (%)	WC-FDM	113.9829	147.4202	140.5684	138.8242	146.1408	0.0186
	Upwind	113.9281	102.4596	13.4014	7.2537	6.4107	3.1637
	Central	239.5639	195.8257	163.8034	169.9778	809.0884	203.1004
	Compact	170.2307	168.4751	165.2753	178.9328	146.1408	0.0186
RRMSE	WC-FDM	0.292123	0.258885	0.182101	0.128184	0.090465	0.000007
	Upwind	0.285254	0.204972	0.023022	0.008397	0.003222	0.001187
	Central	0.547422	0.313837	0.196933	0.143328	0.630505	0.077490
	Compact	0.372421	0.270265	0.207369	0.147175	0.090465	0.000007

TABLE 7. The order of convergence p for the numerical schemes with non-uniform grid spacing.

	Order of convergence p			
Schemes	$\nu = 0.1$	$\nu = 0.05$	$\nu = 0.025$	$\nu = 0.01$
WC-FDM	2.6806	4.3631	3.7274	2.3271
Upwind	0.6351	2.0309	1.5882	1.6845
Central	-0.8459	-1.2630	0.4913	0.3296
Compact	2.6806	4.4664	3.7975	2.3822

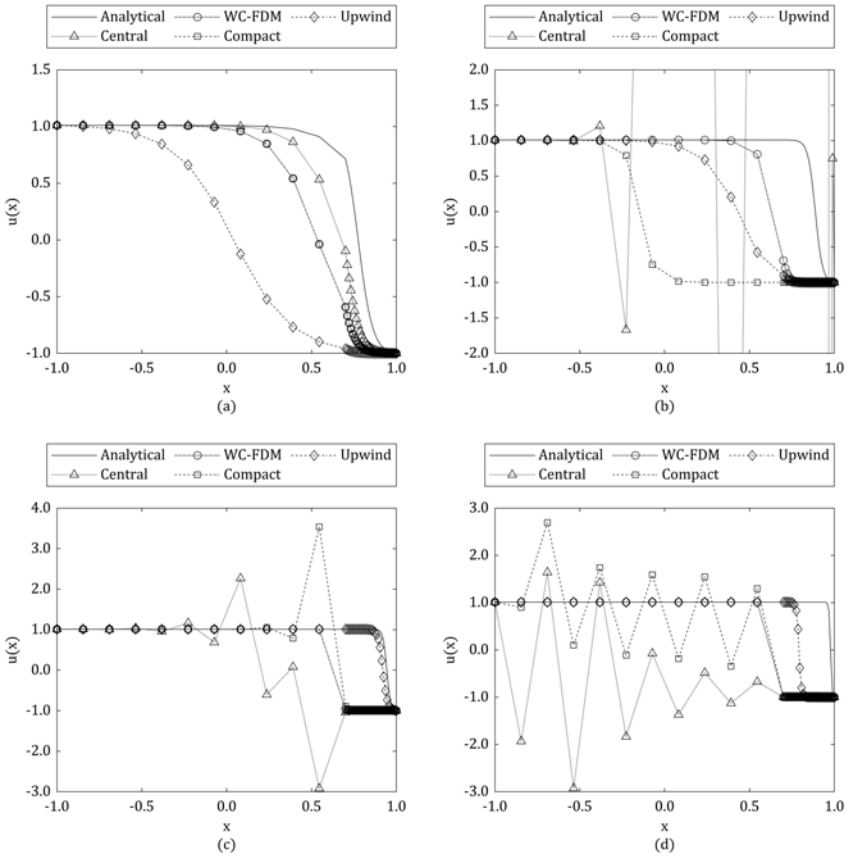

FIGURE 6. Numerical simulation results of the non-linear steady ADE with 40 non-uniformly spaced grid points at different diffusivities a) $\nu = 0.1$, b) $\nu = 0.05$, c) $\nu = 0.025$, and d) $\nu = 0.01$.

8. Conclusion

In this paper, a monotonic weighted finite difference scheme (WC-FDM) is introduced. The proposed WC-FDM scheme is validated against the analytical solution of the non-linear one-dimensional steady advection-diffusion equation (ADE). It is developed to handle both uniform and non-uniform grid spacing. The criteria for selecting weights are demonstrated to ensure the monotonicity of the developed numerical scheme. The computational performance of the proposed WC-FDM scheme is benchmarked against the upwind-central difference scheme, the full central difference scheme, and the fourth-order compact difference scheme.

In the uniform grid spacing scenario, the WC-FDM demonstrates notable advantages over other schemes, particularly in maintaining stability and accuracy across varying diffusivities. It effectively suppresses numerical oscillations in highly advection-dominated situations while preserving accuracy in diffusive contexts. The WC-FDM offers a balance between the advantages of upwind and compact schemes. Conversely, in the non-uniform grid spacing scenario, computational accuracy diminishes across all schemes due to uneven point distribution. As the number of points increases, all schemes converge rapidly, with WC-FDM and compact schemes proving most efficient for high diffusivities, while the upwind scheme excels at low diffusivities. Notably, WC-FDM and compact schemes emerge as the most efficient solutions for all diffusion levels in a non-uniform grid spacing scenario when a very fine stencil size is employed.

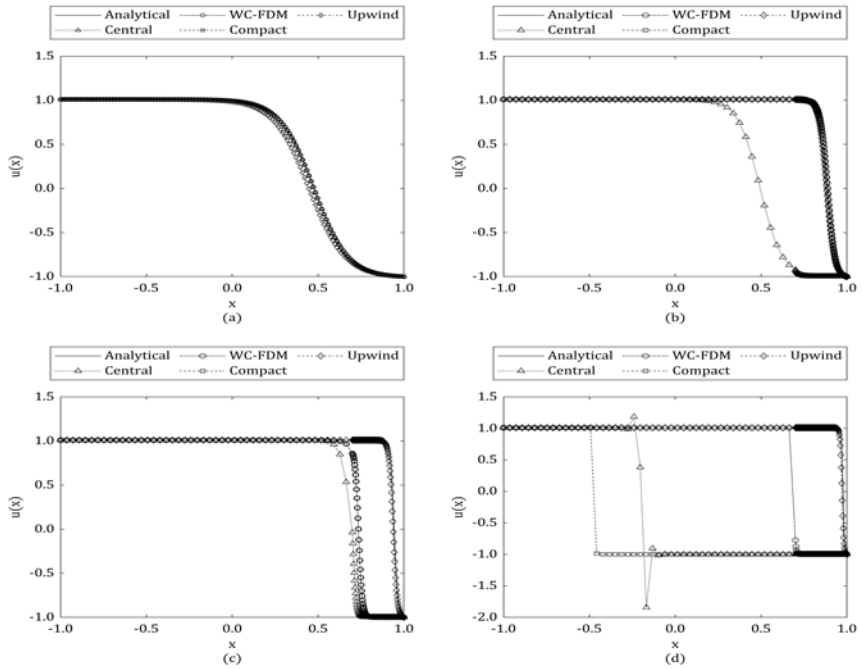

FIGURE 7. Numerical simulation results of the non-linear steady ADE with 160 non-uniformly spaced grid points at different diffusivities a) $\nu = 0.1$, b) $\nu = 0.05$, c) $\nu = 0.025$, and d) $\nu = 0.01$.

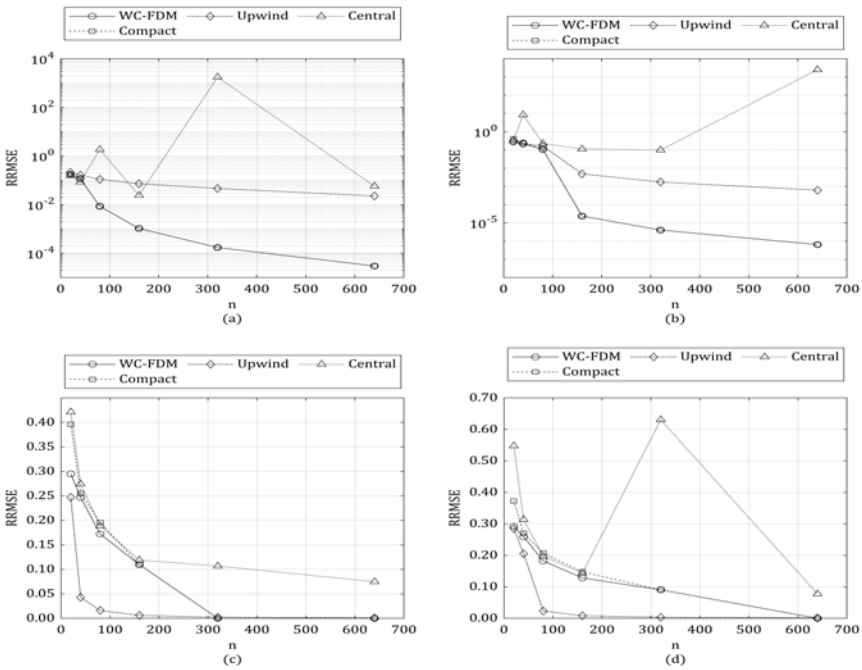

FIGURE 8. Error convergence of the numerical schemes with non-uniform grid spacing at different diffusivities a) $\nu = 0.1$, b) $\nu = 0.05$, c) $\nu = 0.025$, and d) $\nu = 0.01$.

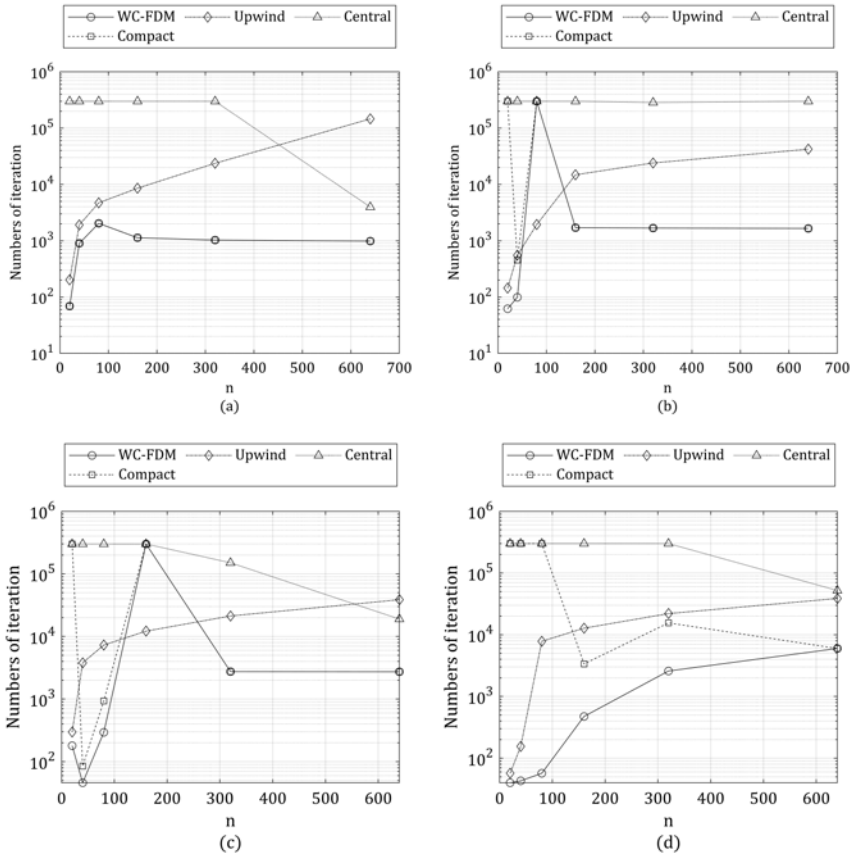

FIGURE 9. Number of iterations of the numerical schemes required to obtain the steady velocity with non-uniform grid spacing at different diffusivities a) $\nu = 0.1$, b) $\nu = 0.05$, c) $\nu = 0.025$, and d) $\nu = 0.01$.

REFERENCES

[1] M. Abdullah, M. Yaseen, and M. D. L. Sen, *An efficient collocation method based on Hermite formula and cubic B-splines for numerical solution of the Burgers' equation*, Math. Comput. Simul., *197* (2022), 166–184.

[2] J. D. Anderson, *Computational Fluid Dynamics: The Basics with Applications*, McGraw-Hill, 1995.

[3] J. B. Angel, J. W. Banks, A. M. Carson, and W. D. Henshaw, *Efficient Upwind Schemes for Linear and Nonlinear Dispersive Maxwell's Equations on Overset Grids*, 2023 International Applied Computational Electromagnetics Society Symposium (ACES), (2023), 1–2.

[4] J. W. Banks and W. D. Henshaw, *Upwind schemes for the wave equation in second-order form*, J. Comput. Phys., *231*(17) (2012), 5854–5889.

[5] S. F. Bradford and N. D. Katopodes, *The anti-dissipative, non-monotone behavior of Petrov–Galerkin upwinding*, Int. J. Numer. Methods Fluids, *33* (2000), 583–608.

[6] H. Charles, *Numerical Computation of Internal and External Flows*, Butterworth-Heinemann, 2007.

[7] P. Chivapornthip, *A Singular Perturbation Solution of Power Law Fluid Flow in Open Channel Tube by Using Quadratic B-spline Collocation Method*, J. Appl. Eng. Sci., *24*(1) (2020), 33 – 41.

[8] L. Corrêa, G. A. B. Lima, M. A. C. Candezano, M. P. S. Braun, C. M. Oishi, H. A. Navarro, and V. G. Ferreira, *A C^2-continuous high-resolution upwind convection scheme*, Int. J. Numer. Methods Fluids, *72* (2013), 1263–1285.

[9] M. Dehghan, *Weighted finite difference techniques for the one-dimensional advection–diffusion equation*, Appl. Math. Comput., *147*(2) (2004), 307–319.
[10] U. Erdogan, *Improved upwind discretization of the advection equation*, Numer. Methods Partial Differ. Equ., *30* (2014), 773-787.
[11] M. E. Fiadeiro and G. Veronis, *On weighted-mean schemes for the finite-difference approximation to the advection-diffusion equation*, Tellus, *29* (1977), 512–522.
[12] H. Karahan, *Solution of Weighted Finite Difference Techniques With the Advection Diffusion Equation Using Spreadsheets*, Comput. Appl. Eng. Educ., *16* (2005), 147–156.
[13] G. V. Krivovichev and S. A. Mikheev, *Stability analysis of schemes with upwind differences for the solution of the system of kinetic equations for the modelling of semi-compressible gas*, International Conference "Stability and Control Processes" in Memory of V.I. Zubov (SCP), (2015), 399–401.
[14] S. Kutluay, A. Esen, and I. Dag, *Numerical solutions of the Burgers' equation by the least-squares quadratic B-spline finite element method*, J. Comput. Appl. Math., *167*(1) (2004), 21–33.
[15] P. W. Li and F. Zhang, *A weighted–upwind generalized finite difference (WU–GFD) scheme with high–order accuracy for solving convection–dominated problems*, Appl. Math. Lett., *150* (2024), 1–7.
[16] W. Liao, *An implicit fourth-order compact finite difference scheme for one-dimensional Burgers' equation*, Appl. Math. Comput., *206*(2) (2008), 755–764.
[17] W. Liao, *A fourth-order finite-difference method for solving the system of two-dimensional Burgers' equations*, Int. J. Numer. Methods Fluids, *64* (2010), 565–590.
[18] P. R. M. Lyra and K. Morgan, *A review and comparative study of upwind biased schemes for compressible flow computation Part I: 1D first-order schemes*, Arch. Comput. Methods Eng., *7* (2000), 19–55.
[19] A. E. Mattsson and W. J. Rider, *Artificial viscosity: back to the basics*, Int. J. Numer. Methods Fluids, *77* (2015), 400–417.
[20] R. C. Mittal and R. K. Jain, *Numerical solutions of nonlinear Burgers' equation with modified cubic B-splines collocation method*, Appl. Math. Comput., *218*(15) (2012), 7839–7855.
[21] T. Öziş and U. Erdoğkan, *An exponentially fitted method for solving Burgers' equation*, Int. J. Numer. Methods Eng., *79* (2009), 696–705.
[22] M. A. Ramadan, T. S. El-Danaf, and F. E. I. A. Alaal, *A numerical solution of the Burgers' equation using septic B-splines*, Chaos Solit. Fractals, *26*(4) (2005), 1249–1258.
[23] B. Saka and İ. Dağ, *Quartic B-spline collocation method to the numerical solutions of the Burgers' equation*, Chaos Solit. Fractals, *32*(3) (2007), 1125–1137.
[24] Y. V. S. S. Sanyasiraju and G. Chandhini, *A note on two upwind strategies for RBF-based grid-free schemes to solve steady convection–diffusion equations*, Int. J. Numer. Methods Fluids, *61* (2009), 1053–1062.
[25] M. Sari and G. Gürarslan, *A sixth-order compact finite difference scheme to the numerical solutions of Burgers' equation*, Appl. Math. Comput., *208*(2) (2009), 475–483.
[26] A. Shaw and D. Roy, *Stabilized SPH-based simulations of impact dynamics using acceleration-corrected artificial viscosity*, Int. J. Impact Eng., *48* (2012), 98–106.
[27] M. Tamsir, N. Dhiman, and V. K. Srivastava, *Extended modified cubic B-spline algorithm for nonlinear Burgers' equation*, Beni-Suef Univ. J. Basic Appl. Sci., *5*(3) (2016), 244–254.
[28] B. J. R. Thornber and D. Drikakis, *Numerical dissipation of upwind schemes in low Mach flow*, Int. J. Numer. Methods Fluids, *56* (2008), 1535–1541.
[29] F. Xiao, X. Tang, and H. Ma, *High-order US-FDTD based on the weighted finite-difference method*, Microw. Opt. Technol. Lett., *45* (2005), 142–144.
[30] S. Xiel, G. Li, S. Yi, and S. Heo, *A compact finite difference method for solving Burgers' equation*, Int. J. Numer. Methods Fluids, *62* (2010), 747–764.
[31] D. Xiu and G. E. Karniadakis, *Supersensitivity due to uncertain boundary conditions*, Int. J. Numer. Methods Eng., *61* (2004), 2114–2138.
[32] X. Yang, Y. Ge, and B. Lan, *A class of compact finite difference schemes for solving the 2D and 3D Burgers' equations*, Math. Comput. Simul., *185* (2021), 510–534.

[33] X. Yang, Y. Ge, and L. Zhang, *A class of high-order compact difference schemes for solving the Burgers' equations*, Appl. Math. Comput., *358* (2019), 394–417.
[34] Y. Yang, M. Li, S. Shu, and A. Xiao, *High order schemes based on upwind schemes with modified coefficients*, J. Comput. Appl. Math., *195* (2006), 242–251.
[35] R. Yeh, Y. S. G. Nashed, T. Peterka, and X. Tricoche, *Fast Automatic Knot Placement Method for Accurate B-spline Curve Fitting*, Comput. Aided Des., *128* (2020), 1–13.
[36] P. G. Zhang and J. P. Wang, *A predictor–corrector compact finite difference scheme for Burgers' equation*, Appl. Math. Comput., *219* (2012), 892–898.